

Visualization of Thalamic Nuclei on High Resolution, Multi-Averaged T_1 and T_2 Maps Acquired at 1.5 T

Sean C.L. Deoni,^{1,2} Melanie J.C. Josseau,² Brian K. Rutt,^{1–3}
and Terry M. Peters^{1–3*}

¹Imaging Research Laboratories, Robarts Research Institute, London, Ontario, Canada

²Department of Medical Biophysics, University of Western Ontario, London, Ontario, Canada

³Department of Diagnostic Radiology and Nuclear Medicine, University of Western Ontario, London, Ontario, Canada

Abstract: The ability to differentiate noninvasively between the primary nuclear divisions of the thalamus has immediate clinical applicability for surgical planning and guidance of functional stereotactic procedures. Comparison of prior qualitative magnetic resonance imaging (MRI) studies carried out at field strengths of 1.5 and 4 Tesla have revealed contrast within the thalamus that varies with field strength, suggesting possible differences in the inherent T_1 and T_2 relaxation times of the constituent nuclei. We investigate this hypothesis through acquisition of high-resolution, multi-averaged deep-brain T_1 and T_2 maps of a healthy volunteer. Fourteen nuclei were identified using their center-of-mass coordinates (in Talairach space) and average T_1 and T_2 values obtained from regions of interest placed within each. Results from this analysis revealed significant differences in T_1 and T_2 between the nuclei with a T_1 range from 700 to 1,400 ms and a T_2 range from 89 to 122 ms, allowing visual discrimination between the major nuclei groups. Furthermore, the high-resolution images showed distinct borders of T_1 and T_2 hypointensity surrounding each nucleus, revealing structure not reported previously. These results confirm our hypothesis and demonstrate the potential high-resolution quantitative imaging for nucleus visualization and surgical planning. *Hum Brain Mapp* 25:353–359, 2005. © 2005 Wiley-Liss, Inc.

Key words: thalamic nuclei; high-resolution imaging; T_1 mapping; T_2 mapping; multi-spectral analysis

INTRODUCTION

In addition to its diagnostic role, magnetic resonance imaging (MRI) has become the modality of choice for surgical planning and image guidance for functional stereotactic neurosurgical procedures, such as the treatment of Parkinson's disease and other motor-control disorders. Patient outcome in these procedures depends on the ability to accurately locate the desired functional region within the thalamus while concurrently avoiding the surrounding anatomy. Although MRI provides excellent contrast between gray matter structures and the surrounding white matter, current qualitative imaging techniques do not provide a high level of contrast within the gray matter structures themselves. This is particularly true within the thalamus, which although containing several functionally distinct

Contract grant sponsor: Canadian Institutes for Health Research; Contract grant number: MT-62716, GR-14973; Contract grant sponsor: Canadian Foundation for Innovation; Contract grant sponsor: University of Western Ontario; Contract grant sponsor: General Electric Medical Systems.

*Correspondence to: Terry M. Peters, Imaging Research Laboratories, Robarts Research Institute, PO Box 5015, 100 Perth Drive, London, ON N6A 5K8, Canada. E-mail: tpeters@imaging.robarts.ca
Received for publication 16 August 2004; Accepted 7 December 2004
DOI: 10.1002/hbm.20117
Published online 25 April 2005 in Wiley InterScience (www.interscience.wiley.com).

regions appears almost homogeneous in most qualitative T_1 - or T_2 -weighted images [Guridi et al., 2000].

Although the use of novel image acquisition strategies such as gray matter nulled inversion recovery [Magnotta et al., 2000] and multi-contrast image fusion [Fletcher et al., 1993] have been investigated to elicit contrast within the thalamus, direct visualization of the individual thalamic nuclei remains a challenge. Consequently, atlases based on anatomic landmarks such as the anterior (AC) and posterior (PC) commissures [Spiegel and Wycis, 1947] and electrophysiologic exploration are necessary for surgical guidance [Finnis et al., 2003; Kirschman et al., 2000]. Unfortunately, anatomic atlases do not fully account for the high degree of anatomic variability between individuals [Van Buren and Borke, 1972] and electrophysiologic exploration can greatly lengthen surgical time. We believe the extent of exploration could be diminished and the efficiency of surgical intervention improved if the preoperative images provided sufficient contrast to allow accurate and reliable differentiation of the thalamic nuclei.

Based on results from prior histologic [Dekaban, 1953; Hassler, 1959] and qualitative MRI investigations [Homes et al., 1998; Magnotta et al., 2000], we hypothesize that structural (fiber size and density) and chemical (myelin and iron concentration) differences between the constituent thalamic nuclei lead to subtle variations in their characteristic longitudinal (T_1) and transverse (T_2) relaxation times. This hypothesis is supported by comparison of high-resolution, multi-averaged T_1 -weighted images of the same individual at 1.5 and 4 Tesla (T) field strengths (shown in Fig. 1), which reveals contrast within the deep brain at 4 T that is not apparent in the 1.5-T images, despite the lower signal-to-noise ratio (SNR) of the 4-T data. These results suggest inherent relaxation time differences within the thalamus that are emphasized at higher field strengths due to the difference in T_1 scaling between the regions. If such differences are indeed present, they should be readily visible on “pure” T_1 and T_2 maps, provided such maps contain sufficient resolution and SNR. Given the spatial complexity of the thalamus, we believe an isotropic spatial-resolution of at least 1 mm^3 is required to adequately resolve the functional nuclei.

In this study, we acquired high spatial-resolution (0.34-mm^3 isotropic voxels) matched T_1 and T_2 maps of the deep brain from a healthy male volunteer. Analysis of these maps demonstrate for the first time subtle variations in the T_1 and T_2 relaxation times among the primary thalamic nuclei, with high T_1 and T_2 ($>1,100$ and >95 ms, respectively) values seen in the medial and posterior nuclei, and lower (~ 950 and 85 ms, respectively) values observed in the lateral and anterior portions of the thalamus. In addition to these large-scale differences, the images also reveal distinct borders of significantly reduced T_1 and T_2 surrounding many of the identified nuclei. Such structure has not been reported previously. These results illustrate the potential of high-resolution quantitative imaging for use in surgical planning and image-guided surgery.

MATERIALS AND METHODS

To map T_1 and T_2 throughout the thalamus and deep brain at high spatial resolution, a set of multi-averaged, high spatial-resolution (0.34 mm^3 isotropic voxels) T_1 and T_2 maps were acquired from a healthy male volunteer using the driven equilibrium single pulse observation of T_1 and T_2 (DESPOT1 and DESPOT2, respectively) quantitative imaging methods [Deoni et al., 2003]. In these methods, T_1 and T_2 information is derived from a series of spoiled gradient-recalled echo (SPGR) and fully balanced steady-state free precession (SSFP) images, allowing acquisition of whole-brain volumetric T_1 and T_2 maps in less than 20 min. In our study, data were acquired using the following imaging parameters: DESPOT1, repetition time/echo time (TR/TE) = $11.4/2.9$ ms, $\alpha = 4$ and 16 degrees, and bandwidth (BW) = ± 7.81 kHz; DESPOT2, TR/TE = $4.2/2.1$ ms, $\alpha = 15$ and 55 degrees, and BW = ± 62.5 kHz. Field of view and matrix size for both sequences were $18 \text{ cm} \times 18 \text{ cm} \times 9 \text{ cm}$ and $256 \times 256 \times 128$, respectively. Total imaging time was approximately 12 min for the T_1 map and 4 min for the T_2 map. To generate high SNR maps, 55 individual T_1 and 25 T_2 maps were independently acquired from the same subject, linearly coregistered, and averaged [Collins et al., 1994; Holmes et al., 1998]. Only 25 T_2 maps were acquired because we have shown previously [Deoni et al., 2003] that optimum T_1 and T_2 precision per unit scan time is achieved when exam time is divided according to the $T_1:T_2$ ratio 75:25. To align the images, rigid-body registration was carried out using an automated 3D approach based on multiscale cross correlation [Finnis et al., 2003].

All data were acquired using a GE (General Electric Medical Systems, Milwaukee, WI) CV/i 1.5-T clinical scanner with a quadrature birdcage headcoil. Informed consent was obtained from the volunteer before scanning and the study was carried out with ethics approval from the Ethics Review Board at the University of Western Ontario.

Average T_1 and T_2 values were determined for the following primary nuclear divisions, where we use the nomenclature of Morel et al. [1997]: dorsomedial (MD), center median (CM), ventral anterior (VA), ventral lateral anterior (VLA), ventral posterolateral (VPL), ventral posteromedial (VPM), the dorsal and ventral divisions of the ventral lateral posterior (VLP), lateral posterior (LP), lateral dorsal (LD), pulvinar (Pul), medial geniculate (MG), lateral geniculate (LG), and the subthalamic nucleus (SThN). The center-of-mass positions (COM) of each of these regions (defined in Talairach space [Talairach et al., 1957]) were mapped onto the T_1 and T_2 maps through appropriate matching of the AC and PC. Mean relaxation time values were calculated from 25 voxel regions of interest (ROIs) placed around each of the COM points. Talairach-defined COM coordinates were used because they represent the “gold standard” locations of the nuclei. T_1 and T_2 values were calculated from small ROIs placed around these points to ensure the points resided within the intended nucleus. A tradeoff was therefore made between including more points, which may have improved our confidence in the nucleus mean T_1 and T_2 values but

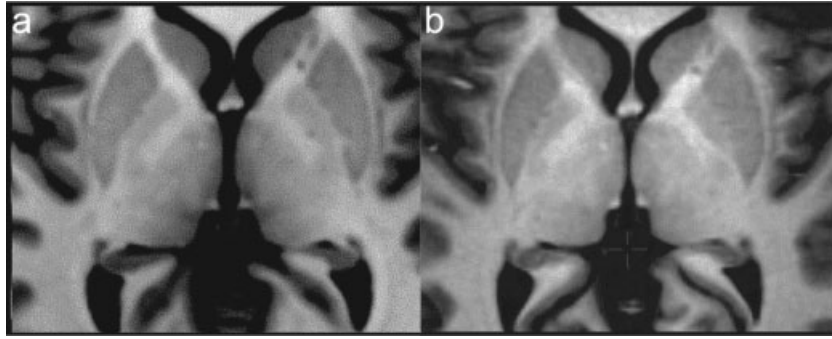


Figure 1.

Comparison of multi-averaged T_1 -weighted images acquired of the same subject at 1.5 T with 27 averages (a) and 4 T with 7 averages (b). Window and leveling has been adjusted in both images to match better the gray/white matter contrast between them. Although the image in a has greater SNR, enhanced thalamic contrast is seen in the 4-T images, suggesting inherent T_1 and T_2 differences in this area.

increased the risk that some of these points lay outside of the intended nucleus.

RESULTS

From the acquired maps, representative coronal and sagittal slices through the mid-thalamus are shown in Figure 2. SNR within the T_1 and T_2 maps (calculated as the mean value of an ROI placed within frontal white matter divided by the standard deviation of the measurements within the ROI) was 33 and 18.7, respectively. Average T_1/T_2 values calculated for white matter (608/54 ms), putamen (1,014/77 ms), caudate nucleus (1,064/89 ms), and globus pallidus (726/55 ms) agree well with published values [Breger et al., 1989], with an average absolute difference of less than 6%. This agreement attests to the accuracy of the DESPOT1 and

DESPOT2 methods and the validity of the measurements obtained from the individual nuclear regions.

To obtain T_1 and T_2 values for each nucleus, ROIs were placed surrounding their 3D Talairach COM coordinates. Average T_1 and T_2 values calculated from these ROIs are illustrated in Figure 3 using a 2D T_1 versus T_2 “feature-space” plot in which the origin of each ellipse represents the mean T_1 and T_2 values obtained from the ROI placed within each nuclei and the major and minor axes represent the standard deviations of the ROI measurements with respect to the T_1 and T_2 measurements, respectively. Results of this analysis demonstrate measurable differences in the inherent T_1 and T_2 relaxation times between the nuclear divisions, with a gradual decrease in both T_1 and T_2 moving from the posterior to anterior and medial to lateral aspects of the thalamus. These results agree well with those observed by

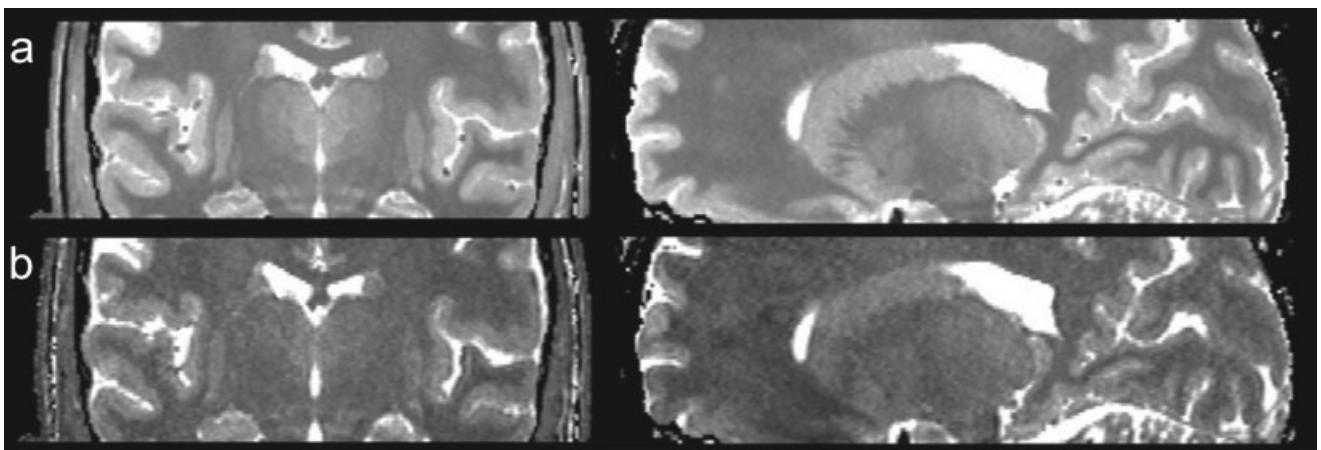


Figure 2.

Representative coronal and sagittal slices through the 3D T_1 map (a) and T_2 map (b) volumes. Average SNRs in the maps were 33 and 19, respectively.

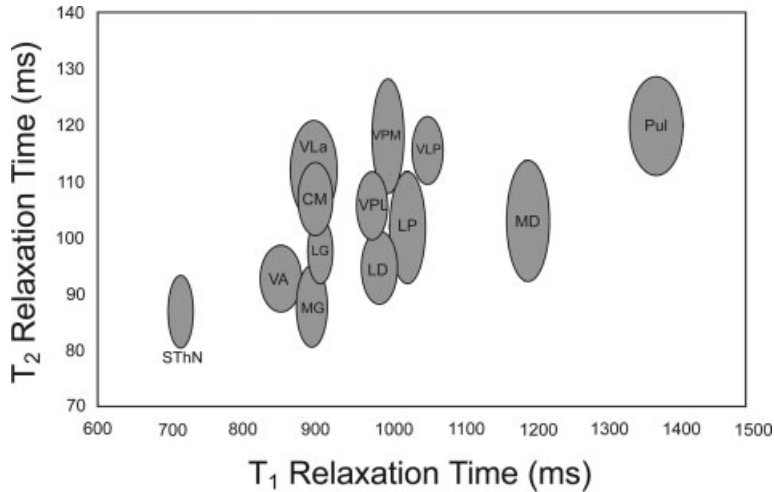


Figure 3. Two-dimensional T_1 vs. T_2 “feature-space” representation of the average T_1 and T_2 values calculated for each nucleus. The origin of each ellipse represents the mean T_1 and T_2 value of the nucleus and the axes represent the standard deviations.

Magnotta et al. [2000] and are consistent with those reported by Holmes et al. [1998].

In addition to these large-scale T_1 and T_2 differences, thin regions of hypointense T_1 and T_2 are noticeable throughout the thalamus, as shown in Figure 4a–e. These regions are emphasized by a manually drawn outline shown in Figure 4f–j. Comparing slices through the T_1 map to representative atlas images (Fig. 5), these seem to outline some of the known nuclear structures and are reminiscent of similar internuclear borders seen on histologic sections stained for cell bodies [Jones, 1985], suggesting these regions may be thin myelin layers or sheaths separating the bodies of the individual nuclei.

DISCUSSION

Prior qualitative imaging studies of the thalamus [Holmes et al., 1998; Lee et al., 1995; Magnotta et al., 2000] have suggested variations in the inherent T_1 and T_2 relaxation times throughout the thalamus, as illustrated in Figure 1. To date, confirmation of such differences has not been carried out, principally due to the long study times associated with quantitative imaging. Underlying reasons for these anticipated relaxation time variations may be deduced by considering the relationships between tissue microstructure and the characteristic T_1 and T_2 . Although water content plays a dominant role in determining T_1 , lipid content also has a strong influence through molecular interactions with the water protons, as well as through the low T_1 of the lipid protons compared to the water protons. Furthermore, the anatomic arrangement of the fibers within each nucleus may also influence T_1 by reducing the number of free water protons [Paus et al., 2003]. Variations in fiber size, density, and myelination are thus expected to yield differences in T_1 between the nuclei. In addition, variations in T_2 may also be anticipated on account of differing densities of oligodendrocytes, the primary iron-containing cell in the brain. As oligodendrocytes play an integral role in myelination, it is reasonable to assume that thalamic regions with increased

myelin will have an associated increase in oligodendrocyte density [Connor and Menzies, 1996], and therefore a decreased T_2 .

We have produced for the first time a set of high spatial-resolution (0.34 mm^3 isotropic voxels) matched T_1 and T_2 maps of the thalamus. Using these data, we have shown measurable differences in both T_1 and T_2 throughout the thalamus on a nuclei-specific basis that agree well with prior observations of signal intensity variations of qualitative T_1 -weighted images. In addition to these large-scale differences, we have also demonstrated thin (approximately 0.7-mm wide) regions of reduced T_1 and T_2 that seem to surround and separate many of the known nuclear divisions. To our knowledge, such observations on in vivo MR images have not been reported previously, although this is likely due to the lower spatial-resolution (greater than 1 mm^3) of conventional qualitative images. Although the possibility exists that these regions are the result of registration error, i.e., through slight misregistration of the multiple data leading to regions of artificially reduced values, the ability to appreciate them in all three dimensions, their consistency between the right and left hemispheres, and their apparent agreement with histologic boundaries suggest that they are anatomically based. Furthermore, these features are reminiscent of similar regions observed on histologic sections stained for cell bodies [Jones, 1985], suggesting that they may be comprised of myelin, which is consistent with their reduced T_1 and T_2 . Further investigation, including in vitro specimen scanning with follow-up histology, is required to determine the structural or chemical mechanism responsible for the reduced T_1 and T_2 in these areas.

The high spatial resolution employed in this study is particularly important for visualizing these hypointense bordering regions. In the images presented here, the regions are approximately 1 pixel (or 0.7 mm) wide and may thus be obscured in parts of the thalamus due to partial volume effects. To reduce this effect and to enhance the visual appearance of these regions, isotropic voxel volumes of less

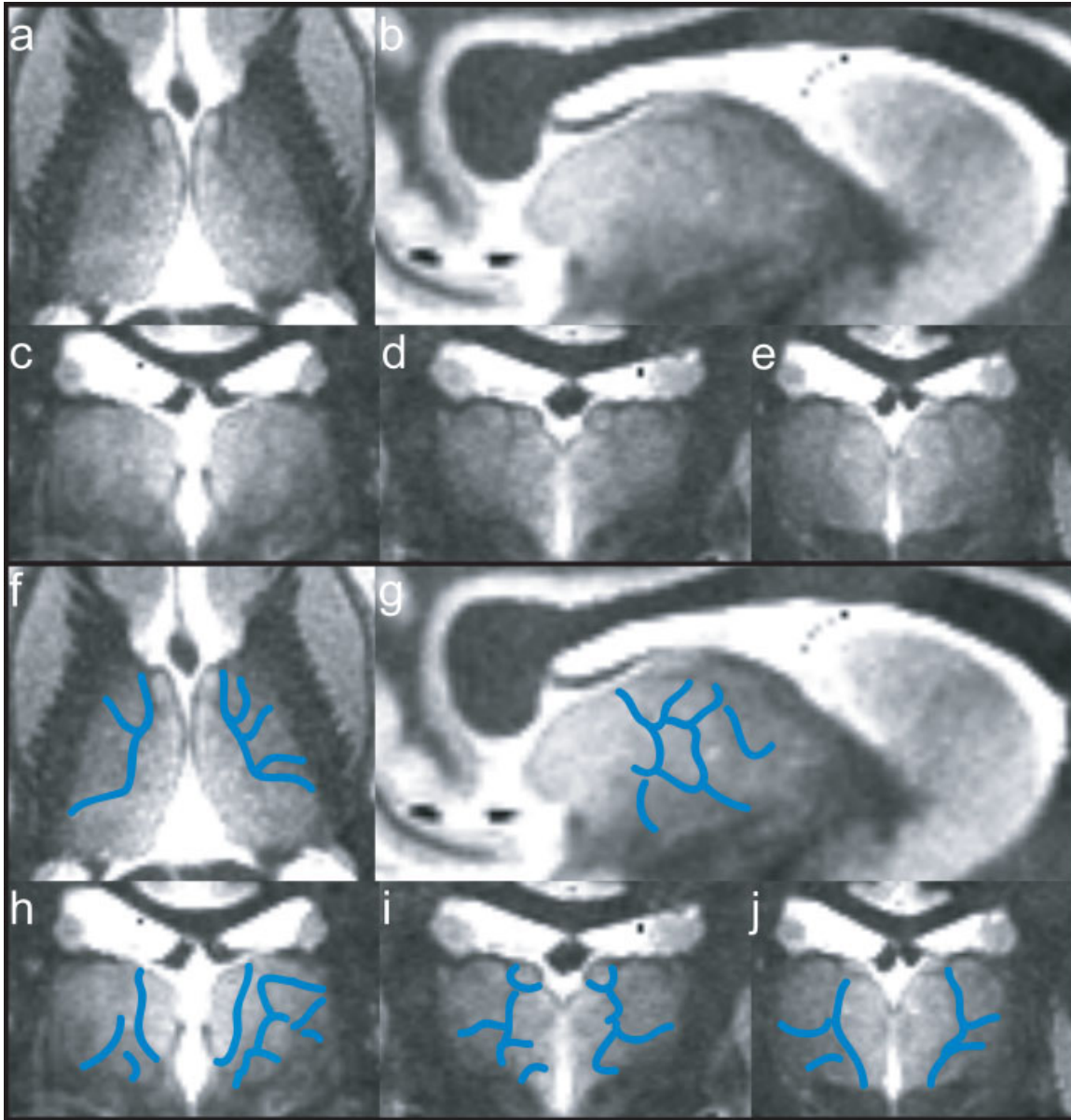


Figure 4.

Axial (a), coronal (b), and sagittal (c–e) slices through the T_1 map volume showing the thin inter-nuclei regions of reduced T_1 (similar observations are made on the T_2 map). To emphasize these thin border regions, f–j show the same images as a–e with these borders manually outlined.

than 0.13 mm^3 (0.5-mm voxel dimensions) would be desirable. To acquire such high spatial-resolution images without sacrificing SNR it would be necessary to move to higher field strength (i.e., 3 T) and employ dedicated, multichannel head coils. Although SNR is anticipated to increase as a result of these measures, a number of challenges are also expected. For both DESPOT1 and DESPOT2, increased inhomogeneity in the excitation RF (B_1) field associated with higher main field strengths will lead to deviations in the flip angle from the expected value, resulting in inaccuracies in the estimated

T_1 and T_2 values. Rapid B_1 mapping will permit correction of these effects.

We have focused on the use of quantitative T_1 and T_2 data to visually identify the thalamic nuclei. Alternative approaches for nuclei delineation presented recently by Wiegell et al. [2003] and Behrens et al. [2003] have made use of fiber orientation data derived from diffusion tensor MRI (DT-MRI). The primary limitation of these approaches is the relatively poor spatial resolution possible with present DT-MRI protocols ($1.8 \text{ mm} \times 1.8 \text{ mm}$ in-plane with 3-mm thick

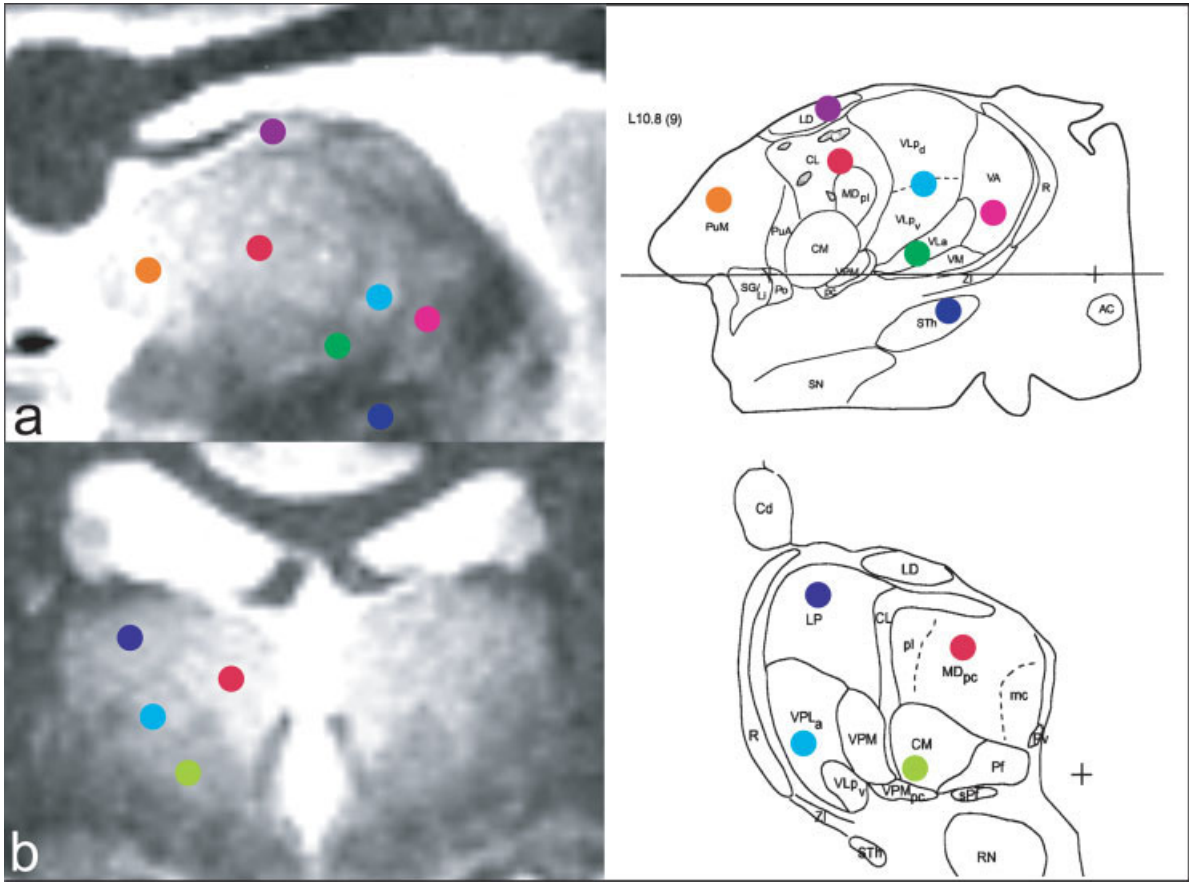


Figure 5.

Comparison of sagittal (a) and coronal slices (b) through the T_1 map with visualized matched slices through the Morel et al. [1997] anatomic atlas. Colored dots are used to identify consistent nuclei. The thin regions of reduced T_1 seem to surround many nuclei and correspond well with the anatomic images.

slices in the case of Wiegell et al. [1003]). This effectively limits these methods from delineating the smaller functional regions of the thalamus. Furthermore, the low anisotropy observed in the thalamus leads to poor estimation of fiber orientations, decreasing the precision of these approaches.

At present, our data consist of 55 T_1 map averages and 25 T_2 maps, representing a clinically unrealistic 13 hr of scanning. The use of dedicated multichannel headcoils accompanied by a move to greater field strength (3 T), is expected to reduce greatly the number of averages and therefore the scan time required. (The use of 3 T coupled with an eight-channel headcoil can be expected to provide a theoretical SNR increase of three to four times in the center of the brain, allowing scan time to be reduced by a factor of 9–16.) Furthermore, as the study represents the first attempt at high-resolution, in vivo quantitative imaging of the deep brain and thalamus, further optimization of the acquisition parameters (i.e., flip angles used) based on the results obtained here is expected to permit further decreases in scan

time, possibly allowing the study to be carried out in a clinical timeframe.

CONCLUSIONS

The ability to visualize noninvasively individual thalamic nuclei has significant clinical potential in surgical planning and image guidance in functional stereotactic neurosurgery. We used high spatial-resolution multi-averaged quantitative T_1 and T_2 imaging to investigate our hypothesis that the structural and chemical differences between the constituent nuclei lead to subtle but measurable differences in their characteristic T_1 and T_2 values. The results presented support this hypothesis and show large-scale differences in both T_1 and T_2 . In addition, we have demonstrated the results have distinct and visible regions of hypointense T_1 and T_2 surrounding many of the nuclei, which have not been reported or demonstrated previously. These results demonstrate the potential and reveal the significant advantages of high-resolution quantitative imaging in identifying and de-

lineating the thalamic nuclei and its future use in surgical planning of minimally invasive surgical procedures in the deep brain.

ACKNOWLEDGMENTS

We thank A. Koziak and Dr. K. Surry for assistance in data collection, Drs. A. Parrent, K. Finnis, and Y. Starreveld for insightful neuroanatomy discussions, and Dr. C. Holmes for providing the 1.5T versus 4T comparison image. B.K. Rutt receives salary support from the Barnett-Ivey Heart and Stroke Foundation of Ontario Endowed Chair award.

REFERENCES

- Behrens TE, Johansen-Berg H, Woolrich MW, Smith SM, Wheeler-Kingshott CA, Boulby PA, Barker GJ, Sillery EL, Sheehan K, Ciccarelli O, Thompson AJ, Brady JM, Matthews PM (2003): Non-invasive mapping of connections between human thalamus and cortex using diffusion imaging. *Nat Neurosci* 6:750–757.
- Breger RK, Rimm AA, Fisher ME, Papke RA, Haughton VM (1989): T1 and T2 measurements on a 1.5T commercial MR imager. *Radiology* 211:489–495.
- Collins DL, Neelin P, Peters TM, Evans AC (1994): Automatic 3D intersubject registration of MR volumetric data in standardized Talairach space. *J Comput Assist Tomogr* 18:192–205.
- Connor JR, Menzies SL (1996): Relationship of iron to oligodendrocytes and myelination. *Glia* 17:83–93.
- Deoni SCL, Rutt BK, Peters TM (2003): Rapid combined T1 and T2 mapping using gradient recalled acquisition in the steady-state. *Magn Reson Med* 49:515–526.
- Dekaban A (1953): Human thalamus; an anatomical, developmental and pathological study. I. Division of the human adult thalamus into nuclei by use of the cyto-myelo-architectonic method. *J Comp Neurol* 99:639–683.
- Finnis KW, Starreveld YP, Parrent AG, Sadikot AF, Peters TM (2003): Three-dimensional database of subcortical electrophysiology for image-guided stereotactic functional neurosurgery. *IEEE Trans Med Imaging* 22:93–104.
- Fletcher LM, Barsotti JB, Hornak JP (1993): A multispectral analysis of brain tissues. *Magn Reson Med* 29:623–630.
- Guridi J, Rodriguez-Oroz MC, Lazano AM, Moro E, Albanese A, Nuttin B, Gybels J, Ramos E, Obeso JA (2000): Targeting the basal ganglia for deep brain stimulation in Parkinson's disease. *Neurology* 35(Suppl):21–28.
- Hassler R (1959): Anatomy of the thalamus. In: Schaltenbrand G, Bailey P, editors. *Introduction of the stereotaxis with an atlas of the human brain*. New York: Gunne & Stratton; p 230–290.
- Holmes CJ, Hoge R, Collins L, Woods R, Toga AW, Evans AC (1998): Enhancement of MR images using registration for signal averaging. *J Comput Assist Tomogr* 22:324–333.
- Jones EG (1985): *The thalamus*. New York: Plenum Press.
- Kirschman DL, Milligan B, Wilkinson S, Overman J, Wetzel L, Batnitzky S, Lyons K, Pahwah R, Koller WC, Gordon MA (2000): Pallidotomy microelectrode targeting: neurophysiology-based target refinement. *Neurosurgery* 46:613–622.
- Lee JH, Garwood M, Menon R, Adriany G, Andersen P, Truwit CL, Ugurbil K (1995): High contrast and fast three-dimensional magnetic resonance imaging at high fields. *Magn Reson Med* 34:308–312.
- Magnotta VA, Gold S, Andreasen NC, Ehrhardt JC, Yuh WT (2000): Visualization of subthalamic nuclei with cortex attenuated inversion recovery MR imaging. *Neuroimage* 11:341–346.
- Morel A, Magnin M, Jeanmonod D (1997): Multiarchitectonic and stereotactic atlas of the human thalamus. *J Comp Neurol* 387:588–630.
- Paus T, Collins DL, Evans AC, Leonard G, Pike B (2003): Maturation of white matter in the human brain: a review of magnetic resonance studies. *Brain Res Bull* 54:255–266.
- Spiegel EA, Wycis HT (1947): Stereotactic apparatus for operations on the human brain. *Science* 106:249–250.
- Talairach J, David M, Tournoux P, Corredor H, Kvasina T (1957): *Atlas d'Anatomic Stereotaxique. Reperage radiologique indirect des noyaux gris centraux des regions mesencephalo-sous-optique et hypothalamique de l'homme*. Paris: Masson et Cie.
- Van Buren JM, Borke RC (1972): *Variations and connections of the human thalamus 2*. New York: Springer-Verlag.
- Wiegell MR, Tuch DS, Larsson HB, Wedeen VJ (2003): Automatic segmentation of thalamic nuclei from diffusion tensor magnetic resonance imaging. *Neuroimage* 19:391–401.